

Research Article

## Hot Water Preparation along with Combined Solar Thermochemical Energy Storage System: Experimental Validation and Performance Simulation

Oleksandr Skrylnyk <sup>†, \*</sup>, Emilie Courbon <sup>†</sup>, Nicolas Heymans <sup>†</sup>, Marc Frère <sup>†</sup>

Department of Thermodynamics and Mathematical Physics, University of Mons, Boulevard Dolez 31, Mons, Belgium; E-Mails: [oleksandr.skrylnyk@umons.ac.be](mailto:oleksandr.skrylnyk@umons.ac.be); [emilie.courbon@umons.ac.be](mailto:emilie.courbon@umons.ac.be); [nicolas.heyman@umons.ac.be](mailto:nicolas.heyman@umons.ac.be); [marc.frere@umons.ac.be](mailto:marc.frere@umons.ac.be)

<sup>†</sup> These authors contributed equally to this work.

\* **Correspondence:** Oleksandr Skrylnyk; E-Mail: [oleksandr.skrylnyk@umons.ac.be](mailto:oleksandr.skrylnyk@umons.ac.be)

**Academic Editor:** Joaquin Alonso-Montesinos

**Special Issue:** [Photovoltaic Solar Systems and Solar Thermal Plants](#)

*Journal of Energy and Power Technology*  
2021, volume 3, issue 2  
doi:10.21926/jept.2102017

**Received:** December 18, 2020  
**Accepted:** March 22, 2021  
**Published:** April 14, 2021

### Abstract

Hybrid solar thermal systems are considered to be a promising solution for delivering clean thermal energy for the building sector, especially while combining them with other renewable energy sources. Usually, solar energy production does not match the thermal energy demand, and hence the energy storage must be integrated. Thermochemical energy storage is adapted particularly to be used along with solar thermal applications. In this article, the design of the combined solar thermochemical energy storage system is presented. The experimental prototype was built and tested within atmospheric conditions. The model of the thermochemical reactor was developed using Matlab<sup>®</sup> and it was validated by the experimental data. The dynamic simulations of the combined solar thermal system for the preparation of domestic hot water were carried out in the TRNSYS environment. The experimental energy storage density of the fully dehydrated material under non-equilibrium conditions was measured between 102 and 158 kWh/m<sup>3</sup>. Dynamic simulations performed in



© 2021 by the author. This is an open access article distributed under the conditions of the [Creative Commons by Attribution License](#), which permits unrestricted use, distribution, and reproduction in any medium or format, provided the original work is correctly cited.

a broader scope of climate conditions showed that the energy storage density in the material under non-equilibrium conditions could vary between 71 and 247 kWh/m<sup>3</sup>.

### Keywords

Thermochemical energy storage; solar system; domestic hot water; composite material

## 1. Introduction

The idea of using thermochemical energy storage based on solid/gas adsorption process in heating and cooling applications gained special attention since the early 90s [1]. The depletion of the ozone layer and global warming were the major driving factors to the onset of the development of solid/gas adsorption technology in heat transforming devices [2]. Initially, the research efforts on the refrigeration cycles having solid/gas adsorption processes dominated over the applications of heat storage and heat generation due to the pre-disposed international legislation brought over on account of the production and consumption of ozone-depleting substances. The adaptation of the world-wide legislation for the promotion of renewable energy production and energy efficiency, along with the decarbonization of the energy sector, resulted in the massive development of various concepts of heat storage systems integrated with the thermochemical process [3].

The solid/gas adsorption principle is based upon the reversible reaction of the gas on the porous solid between the inlet and outlet boundary conditions that are set by temperature and partial pressure. The capturing of gas molecules by a porous solid is an exothermic reaction that is responsible for the heat release, which could be used for immediate heat production. Once the solid/gas equilibrium is attained, the solid must be regenerated to the initial state. Solid regeneration is an endothermic reaction, and it is typically performed by supplying external heat to the solid material. The thermal energy is thus stored in the form of chemical potential.

The integration of thermochemical energy storage in thermal solar systems is one of the effective technological opportunities that deliver clean energy to consumers. Merging the thermochemical process with thermal solar technology is a relatively familiar concept.

However, the commercialization of combined solar thermochemical plants at various scales has not yet reached steady progress. The global technology readiness level oscillates between 5 and 7, while the energy storage costs remain quite high [4]. The ecological aspects, high energy storage density, and the absence of energy loss during the storage period are the biggest advantages of the thermochemical process. Combined small-scale heat storage systems are more suitable for utilization in the residential building sector for space heating and domestic hot water production. These systems are typically operated between 30 °C and 100 °C as boundary conditions.

Fundamentally, thermochemical energy storage concepts for the residential sector are divided into closed systems and open sorption systems. It must be noted that this study considers only concepts concerning the production of domestic hot water or concepts being potentially easily re-configurable for this purpose.

Closed sorption systems usually work under conditions below atmospheric pressure, and the solid material is deposited on the specially designed adsorbent heat exchanger [5]. Roumpedakis et al. studied a solar-driven hybrid adsorption system made for heating and cooling in buildings [6].

The system consisted of 40 m<sup>2</sup> of evacuated tubes solar collectors that were connected to a 12.5 kW zeolite-water adsorption chiller. Researchers reported the great potential that this configuration possessed for the decarbonization of residential energy systems. Wang et al. proposed a hybrid solar adsorption apparatus for water heating and ice-making by using an activated carbon-methanol chemical couple [7]. The experimental apparatus was adjusted to prepare 112-150 kg of hot water at 91.3-98 °C and nearly 10 kg of ice with the help of solar collectors and 22 kg of activated carbon. The coefficient of performance obtained by the prototype was close to 0.4, and the system efficiency varied between 76% and 90%. Ji et al. developed a solar, hot water-driven, vacuum adsorption system for making ice using activated carbon-methanol as a working pair [8]. The ice-making capacity of the prototype was 8.4 kg per day, with the lowest temperature reaching - 8.4 °C and hot water temperature maintained at 94 °C. The best coefficient of performance was recorded as high as ~0.14, and the system heat utilization efficiency was close to 54%. Zhao et al. designed a closed sorption heat storage apparatus for the preparation of domestic hot water using lithium chloride-water chemical couple [9]. The energy storage density of the sorption device was nearly 65 kWh/m<sup>3</sup> at charging and discharging temperatures of 85 °C and 40 °C, respectively. The total heat storage efficiency was as high as 94%.

Concerning open sorption systems, the design is generally limited to the use of humid air. This type of system consists of open inlet and outlet boundaries, with the flowing humid air being in direct contact with the solid [10]. For such systems, the exothermic reaction leads to material hydration, while the dehydration of the material is achieved by an endothermic reaction. Gaeini et al. constructed open sorption, multi-modular, thermochemical energy storage for domestic hot water production using a zeolite-water working pair [11]. The average experimental energy storage density was 108 kWh/m<sup>3</sup> at the reactor scale with charging and discharging temperatures of 190 °C (hot air) and 10 °C (outdoor humid air). The average combined thermal power output was nearly 3.6 kW at a period of 10 h. The following examples describe space heating systems that could be potentially converted to produce domestic hot water. Michel et al. developed large-scale, open sorption, thermochemical energy storage for building heating that consisted of a stack of packed beds filled with 400 kg of hydrated strontium bromide [12]. The prototype was able to store up to 105 kWh, and its energy storage density was 203 kWh/m<sup>3</sup>. Aydin et al. tested a prototype of an open sorption modular reactor for solar thermal energy storage [13]. The authors focused on the evaluation of the vermiculite-calcium chloride composite material reacting with humid air. The energy storage density on the material scale varied from 33 to 100 kWh/m<sup>3</sup> depending on the air humidity and the inlet air temperature, which was set between 14 °C and 21 °C. The average thermal power output of the reactor varied between 313 W and 730 W.

These examples give a general idea about the performance characteristics of various thermochemical energy storage devices used with solar thermal systems. The choice of the technology used (closed or open sorption reactor) is mostly determined by the working pair, targeted application (heat storage or heat transformation), and the time scale between energy charging and discharging. However, the differences in the techno-economic performances between the closed and open sorption systems are not as significant as shown in studies by Scapino et al. [4], and Bertsch et al. [14]. Moreover, the comparison of performance characteristics for various systems presented in the literature is difficult to be carried out due to the lack of a common calculation methodology for the key performance indicators, as discussed by Palomba et al. [15].

In this article, a combined solar thermal system with open sorption, thermochemical energy storage is designed and validated. The combined system is dedicated to the preparation of domestic hot water in residential buildings. The novelty of the work consists of the following. First, the intermediate scale prototype of the thermochemical energy storage system was built and experimentally tested by using the recently developed composite solid adsorbent. Second, the experimental data were used to validate the mathematical model of the thermochemical reactor. The apparent kinetic coefficient was represented by the grey-box model along with a sigmoid-shaped function. Finally, the in-depth study of the dynamic behavior of the combined solar energy system with an account of the consumption profile of domestic hot water was conducted by using the numerical simulation approach in the TRNSYS environment for the daily and typical climatic conditions in Brussels (Belgium). The lead-off automation algorithm was proposed to study the dynamic behavior of the combined solar system. This article contributes to the design of the thermochemical energy storage devices coupled to the solar thermal systems present in residential buildings. The results of the work are helpful to bridge the gap in the academic knowledge concerning the integration of thermochemical energy storage to hybrid heating systems.

## 2. Materials and Methods

### 2.1 Thermochemical Energy Storage

The combined solar energy system integrates thermochemical energy storage, and it is primarily designed for the preparation of domestic hot water in a residential building. As the production of hot water is mainly due to the adsorption process, the study of the system configuration was adjusted in this mode. The desorption mode was not included in the present study. The system's design in the adsorption mode is shown in Figure 1. Conceptually, the system consists of an array of solar thermal collectors (1), a hot water storage tank (2), a modular open sorption thermochemical reactor (3), and a back-up thermal device (4). Under ideal conditions, the working principle of the combined system is as follows. During a period of low solar irradiance, the water storage tank (2) is heated up by the adsorption process (3) until all the adsorbent beds (modules) reach a hydrated state and no further significant heat generation by the exothermic reaction is possible. To do this, first, the outside cold and humid air at a temperature  $T_a$  is pre-heated through the heat exchanger  $HX_2$ . Afterward, the warm and humid air is blown constantly from the heat exchanger  $HX_2$  to the reactor (3) through the fan  $F_1$ . The reaction heat is used to charge the water tank (2) through the air-to-water heat exchanger  $HX_1$ . The expected charging temperature of the water tank ranges from 40 °C to 50 °C, which roughly allows the energy storage density in the material to be between 120 kWh/m<sup>3</sup> and 150 kWh/m<sup>3</sup>. The air-to-air heat exchanger  $HX_2$  is also used for heat recovery; thus, it allows the rejected reaction heat to be re-injected to the heating process. During the period of high solar irradiance, the charge of the water storage tank (2) is continued by the array of solar thermal collectors (1) until the water temperature reaches a usable level between 60 °C and 90 °C. By default, the solar thermal collectors are glazed flat plate collectors. However, evacuated tubes or concentrated solar thermal collectors can be plugged too. The back-up thermal device (4) is only used in case of a mismatch ( $T_{DHW,out} < T_{DHW}^0$ ) of the tank outlet temperature  $T_{DHW,out}$  with the reference temperature profile of the user  $T_{DHW}^0$ . The working cycle of the hydraulic pump  $P_1$  is controlled by the solar thermal collectors, while the hydraulic pump  $P_2$  is simultaneously activated or disabled with the fan  $F_1$ .

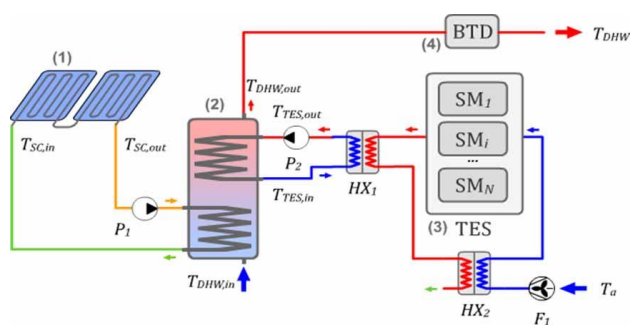


**Figure 1** Combined solar thermal system with thermochemical energy storage.

The thermochemical reactor (3) is assembled from removable storage modules  $SM_i, i = \overline{1 \dots N}$  each filled with solid adsorbent. The modules are stacked horizontally, and they are assembled in such a way that the inlet air flows in a cross-sectional direction through the surface area of each of the modules. Modules with hydrated solid are replaced by the modules with dehydrated material that is available in the stock. Conceptually, each storage module is designed as a rectangular tray with dimensions  $L \times W \times H$ , respectively representing the module's length, width, and depth. The solid adsorbent is confined between the tightly stretched upper and lower metallic sieves. The schematic presentation of a storage module is shown in Figure 2.

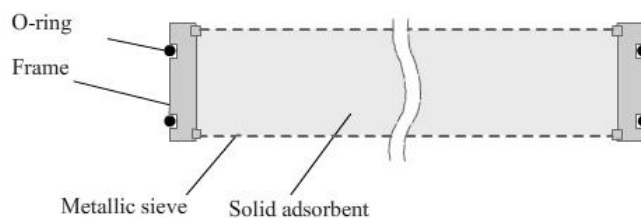


**Figure 2** Schematic representation of the storage module.

## 2.2 Solid Adsorbent

The solid adsorbent used in this procedure is a composite material that reacts with water vapor. The composite material consists of a mesoporous matrix having trapped salt of calcium chloride ( $\text{CaCl}_2$ ). The mesoporous matrix is the Davisil<sup>®</sup> silica gel (grade 62) from Grace. The  $\text{CaCl}_2$  was supplied by Solvay in the form of anhydrous Caso<sup>®</sup> granulate. This composite was developed at the Research Institute for Energy at the University of Mons (Belgium), and it was tested with various sample scales in prototype installations as reported by Skrylnyk et al. [16] and Wyttenbach et al. [17]. This composite adsorbent was synthesized using a patented multi-step wetness incipient impregnation method. This method allowed a high salt content to be reached (43 wt.%) inside silica gel. A detailed description of the synthesis procedure has been given by Courbon et al. [18]. Afterward, the synthesized sample was characterized by commonly used methods. The reaction heat was determined from the thermal gravimetric and differential scanning calorimetric analysis using TGA/DSC 111, which was connected to the Wetsys humidifier from Setaram. The water adsorption isotherms were obtained from dynamic vapor sorption tests using IGASorp from Hiden Isochema. The porous characteristics were measured using nitrogen sorption measurements at 77 K by using Belsorp-max from BEL-Japan. The total volume of the pores was determined at  $p_v/p_v^0 =$

0.99, while the specific surface area was obtained by the Brunauer-Emmett-Teller method. The properties and characteristics of this composite adsorbent are presented in Table 1. The water adsorption isotherms are shown in Figure 3.

**Table 1** Characteristics of the silica-CaCl<sub>2</sub> composite adsorbent [18].

Characteristic	Value
Reaction heat (kJ/kg <sub>H<sub>2</sub>O</sub> )	2757
Total volume of the pores (cm <sup>3</sup> /g)	0.38
Specific surface area (m <sup>2</sup> /g)	75
Packing density of anhydrous material (kg/m <sup>3</sup> )	703
Average particle size (μm)	390

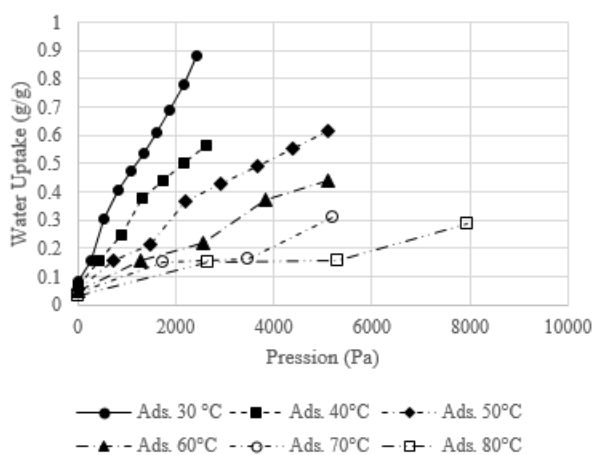


**Figure 3** Water adsorption isotherms of water sorption on the silica-CaCl<sub>2</sub> composite material [18].

### 2.3 Experimental Procedure

The collection of experimental data for the adsorption mode was performed in a prototype installation, whose design slightly differed from the original concept, which was presented in Figure 1. The scale of the experimental prototype was also adjusted to study the adsorption mode. The reactor (3) consisted of a single storage module with a capacity to hold 2.5 kg of solid. The volume of the water storage tank was 50 L. The airflow rate of the fan was set to 100 m<sup>3</sup>/h. No solar collectors or back-up thermal devices were used. The water was not consumed from the tank during thermal charge. The storage module was fully instrumented, and it was mounted inside a metallic housing. The instrumentation scheme of a single storage module is shown in Figure 4. The geometric data of the storage module are presented in Table 2, and the technical characteristics of measuring instruments are presented in Table 3.

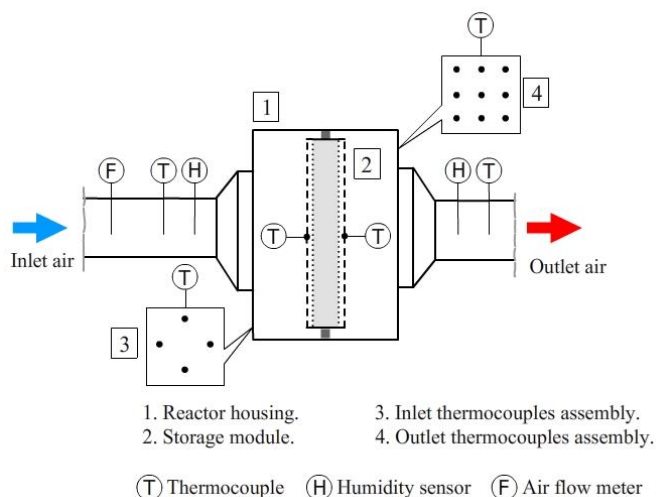


**Figure 4** Instrumentation of a single storage module.

**Table 2** Size characteristics of the experimental storage module.

Characteristic	Value
Width (m)	0.60
Length (m)	0.52
Depth (m)	0.01
Capacity (kg)	2.5
Volume (m <sup>3</sup> )	$3.12 \times 10^{-3}$

**Table 3** Technical characteristics of the measuring equipment.

Instrument	Precision	Range
Thermocouple standard, type K	0.75 %	-270 – 1370 °C
Humidity sensor, VAISALA HMP5	± 0.8 % RH. at 40 – 95 % R.H.	0 – 100 % R.H., -70 – 80 °C
Air flow meter, HÖNTZCH FA ZS30	± 0.01 m/s	0.3 – 2 m/s
Water flow meter, NATEC FT2	< ± 0.07 l/min	0.15 – 4.5 l/min

The experimental procedure was as follows: first, the composite was dehydrated in an oven at 150 °C for 24 h. Then the composite was loaded in the storage module inside the reactor. Afterward, the composite was hydrated for approximately 1 h ( $t_{max}$ ) by blowing ambient humid air through the reactor. The experimental data of the temperature and humidity at the inlet and outlet of the reactor, as well as the temperature on both sides of the storage module (see Figure 4), were recorded in the computer using the data acquisition system CompactDAQ from National

Instruments. Finally, the following treatment procedure was applied to the measured data. The calculation of the water uptake was done with the following formula:

$$x_s(t) = \frac{1}{m_s} \int_{t_0}^{t_{max}} \dot{m}_a \cdot \Delta w_v(t) dt \quad (1)$$

Here,  $m_s$  is the mass of the solid in the storage module,  $\dot{m}_a$  is the dry air mass flow rate, and  $\Delta w_v = w_{v,out} - w_{v,in}$  is the difference between air humidity measured at the inlet  $w_{v,in}$  and outlet  $w_{v,out}$  of the reactor. The thermal power produced at the reactor's boundaries was determined as follows:

$$\dot{Q}_a(t) = \dot{m}_a C_{P,a} \cdot \Delta T_a(t) \quad (2)$$

$C_{P,a}$  is the thermal capacity of the dry air,  $\Delta T_a$  is the variation in air temperature measured between the inlet and outlet of the reactor. Note that equation (2) refers to the sensible heat flow added in the air by the adsorption reaction. It was also considered that the water present in the water storage tank was heated via the heat exchanger  $HX_1$  thanks to the sensible heat. No condensation occurred in the heat exchanger  $HX_1$  during thermal charge.

Thermal energy produced by the reactor was calculated by the following formula:

$$E_r = \int_{t_0}^{t_{max}} \dot{Q}_a(t) dt \quad (3)$$

Energy storage density at the material scale was determined from the following relation:

$$\Delta E_r = \rho_s \frac{E_r}{m_s} \quad (4)$$

Here  $\rho_s$  is the volumetric mass of the anhydrous composite.

## 2.4 Modeling and Simulation Methods

### 2.4.1 Reactor Modeling

The modeling of the reactor is based on the following considerations. Given, a micro-granular porous solid consisting of spherical particles of the same diameter  $d_p$  is packed in a one-dimensional bed having a height  $L_{bed}$  and width  $d_{bed}$ . The humid air flows with a constant linear velocity  $u_g$  through the porous solid in the direction perpendicular to the surface area of the bed. The one-dimensional packed bed is presented in Figure 5. The effects of the radial dispersion of the carrier gas (dry air) in a porous medium are neglected in the model.

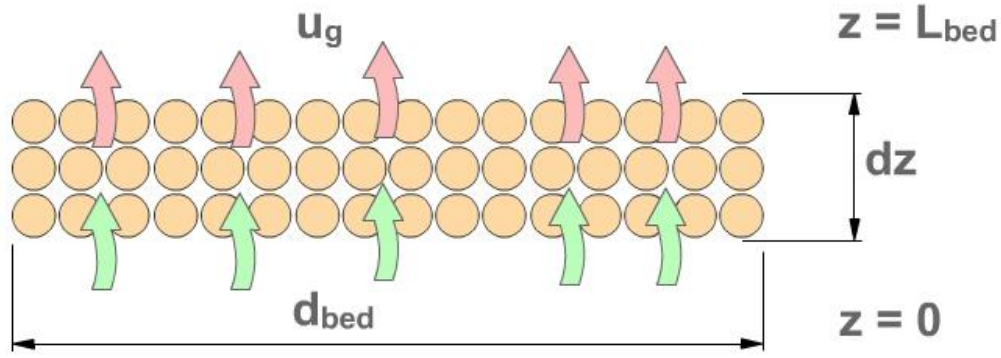


**Figure 5** Presentation of a packed adsorption plate for reactor modeling.

The adsorption of water vapor on the composite is modeled by a set of the following mathematical equations. The mass balance of the humidity content  $w_v$  in the flowing air is written as follows:

$$\rho_a \frac{\partial w_v}{\partial t} + \frac{\partial}{\partial z} (u_g \rho_a w_v) = D_L \rho_a \frac{\partial^2 w_v}{\partial z^2} + (-1) \cdot \rho_s \cdot \left( \frac{1 - \varepsilon}{\varepsilon} \right) \cdot \frac{\partial x_s}{\partial t} \quad (5)$$

Here,  $D_L$  is the diffusivity of the water vapor along the  $z$  axis.

The variation of the temperature of humid air  $T_g$  flowing through the porous medium along the  $z$  axis is written as follows:

$$\rho_g C_{p,g} \frac{\partial T_g}{\partial t} + \frac{\partial}{\partial z} (u_g \rho_g C_{p,g} T_g) = \lambda_L \frac{\partial^2 T_g}{\partial z^2} + h_0 \frac{6}{d_p} \cdot \left( \frac{1 - \varepsilon}{\varepsilon} \right) \cdot (T_s - T_g) \quad (6)$$

With  $\lambda_L = D_L C_{p,g} \rho_g$  being the thermal diffusivity and  $h_0$  being the heat transfer coefficient. Equations (5) and (6) are coupled to the following mass and heat balance equations (7) and (8) in the solid medium. The variation of the water uptake  $x_s$  in solid is modeled by the following equation:

$$\frac{\partial x_s}{\partial t} = k_o (x_s^0 - x_s) \quad (7)$$

Here,  $k_o$  is the kinetic coefficient and  $x_s^0 = x_s^0(T_s, p_v)$  is the water uptake under equilibrium conditions, which is determined from the isotherm characteristics, and which depends on the adsorption temperature  $T_s$  and water vapor pressure  $p_v$ . The variation in temperature  $T_s$  in a solid material is determined by the following energy balance equation:

$$\rho_s (C_{p,s} + C_{p,w} x_s) \frac{\partial T_s}{\partial t} = h_0 \frac{6}{d_p} \cdot (T_g - T_s) + \rho_s \frac{\partial x_s}{\partial t} \cdot \Delta H_s \quad (8)$$

Here  $\Delta H_s$  is the reaction heat, which is equal to 2757 kJ/kg (see Table 1). The boundary conditions complete the adsorption model expressed by equations (5-8). In the present model, the Danckwerts boundary conditions are considered as discussed by Pearson's [19]. The conditions for mass transfer of humid air at the geometric boundaries are written as follows:

$$\begin{aligned}
 -D_L \frac{\partial(\rho_a w_v)}{\partial z} &= u_g \rho_a w_{v,in} - u_g \rho_a w_v, & z = 0^+ \\
 -D_L \frac{\partial(\rho_a w_v)}{\partial z} &= 0, & z = L_{bed}
 \end{aligned}
 \tag{9}$$

The conditions for energy flow through the bed boundaries are set by the following equations:

$$\begin{aligned}
 -\lambda_L \frac{\partial T_g}{\partial z} &= u_g C_{p,g,in} \rho_g T_{g,in} - u_g C_{p,g} \rho_g T_g, & z = 0^+ \\
 -\lambda_L \frac{\partial T_g}{\partial z} &= 0, & z = L_{bed}
 \end{aligned}
 \tag{10}$$

The heat transfer coefficient  $h_0$  can be determined from the Nusselt number  $Nu = h_0 d_p (\lambda_g)^{-1}$ , where the Nusselt number is calculated using the following correlation given by Wakao et al. [20]:

$$Nu = 2 + 1.1 Re^{\frac{2}{3}} Pr^{\frac{1}{3}}
 \tag{11}$$

The thermal conductivity of the humid air is modeled using the Sutherland-Thiesen equation for binary mixtures as discussed by Buddenberg et al. [21]:

$$\lambda_g = \sum_{i=\{a,v\}} \frac{\lambda_i}{1 + a_i X_m}
 \tag{12}$$

Here,  $X_m$  is the molar fraction of the moisture present in the air, which is given as  $X_m = x_v M_a (M_v)^{-1}$ , and  $a_i, i = \{a, v\}$  is the coefficient in the Sutherland-Thiesen equation being determined, respectively for dry air ( $a$ ) and water vapor ( $v$ ) as follows:

$$a_i = \frac{1}{4} \left( 1 + \left( \frac{\mu_i}{\mu_j} \cdot \left( \frac{M_i}{M_j} \right)^{\frac{3}{4}} \cdot \frac{1 + \frac{S_i}{T_g}}{1 + \frac{S_j}{T_g}} \right)^{\frac{1}{2}} \right)^2 \cdot \left( \frac{1 + \frac{S_{av}}{T_g}}{1 + \frac{S_i}{T_g}} \right)
 \tag{13}$$

With  $\mu_{\{i,j\}}$  is the dynamic viscosity of each component in the binary mixture,  $M_{\{i,j\}}$  is the molar mass of each component, and  $S_{\{i,j\}}$  is the Sutherland constant. It must be noted that index  $j = \{v, a\}$  represents the permutation of the set  $i$ . The Sutherland constants for dry air and water vapor  $S_a = 111 \text{ K}$ ,  $S_v = 961 \text{ K}$  and  $S_{av} = 0.733 \sqrt{S_a S_v}$ .

The kinetic coefficient was identified from the experimental data using the following empirical relation (sigmoid-shaped function):

$$\hat{k}_o = b_0 \cdot [1 - \text{atan}((x_s - b_1) \cdot b_2) b_3]
 \tag{14}$$

The relation (14) can be written in general form as follows:

$$\hat{k}_o = \hat{K} \cdot F(x_s)
 \tag{15}$$

where  $\hat{K}$  is the characteristic kinetic coefficient at the characteristic water uptake  $x_s = b_1$ . The characteristic kinetic coefficient is defined by the parameter  $b_0$ .  $F(x_s)$  is the saturation-like correction term,  $F(x_s) \in \mathbb{R}^+$ , whose value is equal to  $F(x_s) = 1$  as the characteristic water uptake  $x_s = b_1$ . The characteristic water adsorption uptake is defined at a hydration level, in which significant changes in the water sorption mechanism occur.

The model parameters  $b_k, k = 0 \dots 3$  in equation (14) were found by solving the following parametric identification problem:

$$\min \left( \sum_{l=1}^N (\hat{k}_{o,l}(b_k) - \bar{k}_{o,l})^2 \right), \quad (\forall \hat{k}_{o,l}, \forall \bar{k}_{o,l}) \in \mathbb{R}^+ \quad (16)$$

where  $\bar{k}_{o,l}$  is the experimental kinetic coefficient that was estimated for each  $1 \leq l \leq N$  point in the measured datasets:

$$\bar{k}_{o,l} = \frac{\dot{m}_a \cdot \Delta w_v}{m_s \cdot (x_s^0(T_{g,out}, \bar{p}_v) - x_s)} \quad (17)$$

where  $m_s$  is the mass of anhydrous solid,  $x_s$  is estimated from the experimental data and with air humidity difference  $\Delta w_v$  between the inlet and outlet of the reactor. It was hypothesized that the thermodynamic equilibrium  $x_s^0$  depends on the average water vapor pressure between the inlet and outlet conditions of the reactor  $\bar{p}_v = \frac{1}{2} \cdot (p_{v,in} + p_{v,out})$  and that there is a thermal equilibrium between solid and gas in the outlet conditions  $T_{g,out} \equiv T_s$ .

#### 2.4.2 Combined Solar System Simulation

In this study, the dynamic behavior of the combined solar system shown in Figure 1 was simulated in the TRNSYS environment. Firstly, the numerical model of the adsorption process described by the equations (6-10) was created using Matlab® software. Secondly, this model was integrated as a separate component in the simulation environment of the TRNSYS software. Finally, the technical components (*e.g.*, reactor, heat exchangers, solar thermal collectors, water storage tank) were linked to recreate the combined solar energy system shown in Figure 1. The climate data were linked to the boundary conditions of the reactor and other technical components. The principal scheme for the simulation of the system is provided in Figure 6.

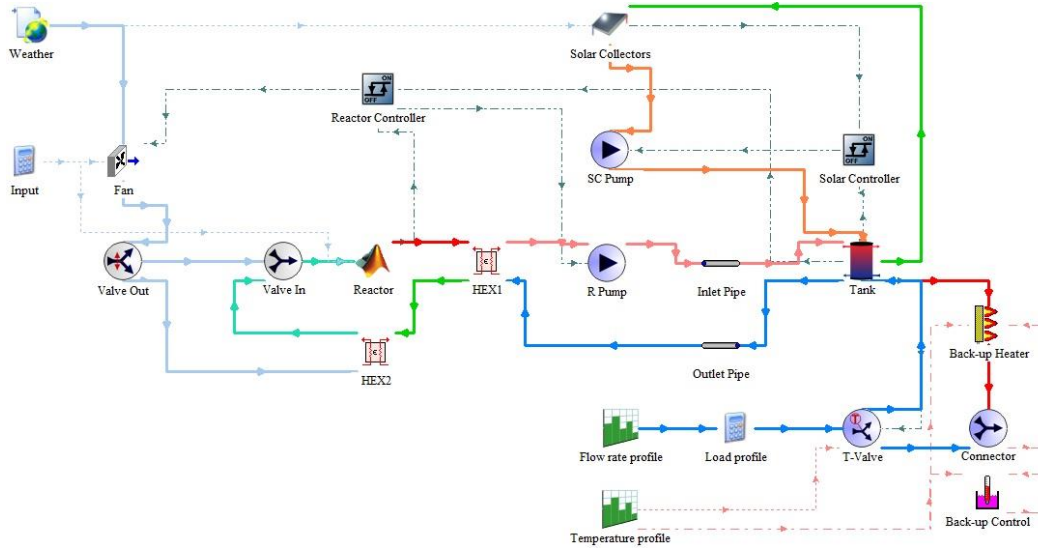


**Figure 6** Principal scheme of the combined solar system for the simulation in the TRNSYS environment.

The complete control of the combined solar energy system is ensured by the elements denoted as ‘Reactor Controller’ and ‘Solar Controller’ as shown in Figure 6. The ‘Reactor Controller’ is used to switch on and off the ‘Fan’ and the ‘R Pump’ using the signals from the ‘Reactor’ and the ‘Tank’, while the ‘Solar Controller’ comprehends a typical on/off control of the ‘SC Pump’ in the outlet circuit of the solar collector. Additionally, the element ‘Back-up Control’ is used to switch on the ‘Back-up Heater’ in case the tank outlet temperature  $T_{DHW,out}$  is below the reference temperature  $T_{DHW}^0$ . The control algorithm is described by the following logical relations. The reactor is switched on by the following condition:

$$\gamma_r = \begin{cases} 1, & (w_{v,in} \geq w_v^{min}) \wedge (T_{a,in} \geq T_a^{min}) \wedge (\bar{T}_{DHW} < T_{DHW}^{max}) \\ 0, & (w_{v,in} < w_v^{min}) \vee (T_{a,in} < T_a^{min}) \vee (\bar{T}_{DHW} \geq T_{DHW}^{max}) \end{cases} \quad (18)$$

Where  $\bar{T}_{DHW}$  is the average temperature of the storage tank,  $w_v^{min}$  is the minimal cut-off air humidity,  $T_a^{min}$  is the minimal cut-off air temperature, and  $T_{DHW}^{max}$  is the maximum admissible charging temperature of the storage tank by the thermochemical modular system. The storage modules in the reactor are replaced under the following condition:

$$\gamma_s = \begin{cases} 1, & (T_{a,out} < \bar{T}_{DHW} + \Delta T_{bl}) \wedge (\bar{x}_s > x_s^{min}) \\ 0, & (T_{a,out} \geq \bar{T}_{DHW} + \Delta T_{bl}) \vee (\bar{x}_s \leq x_s^{min}) \end{cases} \quad (19)$$

Here,  $T_{a,out}$  is the air temperature at the outlet of the reactor,  $\Delta T_{bl}$  is the switching hysteresis,  $\bar{x}_s$  is the average water uptake for all storage modules in the reactor, and  $x_s^{min}$  is the minimal water uptake, which allows the solid to be replaced.

The heat from the solar collectors is charged to the hot water storage tank by using the typical control law of the domestic solar thermal systems, which is provided as follows:

$$\gamma_{SC} = \begin{cases} 1, & (T_{SC,in} < T_{SC,out}) \wedge (T_{SC,in} < T_{SC}^{max}) \\ 0, & (T_{SC,in} \geq T_{SC,out}) \vee (T_{SC,in} \geq T_{SC}^{max}) \end{cases} \quad (20)$$

$T_{SC}^{max}$  is the cut-off temperature for the solar thermal collectors. Additionally, the back-up thermal device is activated by the following control law:

$$Y_{BTD} = \begin{cases} 1, & T_{DHW,out} < T_{DHW}^0 \\ 0, & T_{DHW,out} \geq T_{DHW}^0 \end{cases} \quad (21)$$

### 3. Results and Discussion

#### 3.1 Validation of Reactor Model

The validation of the reactor model was completed within two stages. During the first stage, the hydration experiments were performed within the prototype installation using a single storage module (see Figure 4). The experimental data were recorded and treated by the procedure described in Section 2.3. During the second stage, the model parameters were determined. The heat transfer coefficient  $h_0$  was calculated using the relations (11-13). Its value was identified to be invariable and equal to  $524 \pm 3 \text{ W K}^{-1} \text{ m}^{-2}$ . The kinetic coefficient  $k_0$  was identified *a posteriori* from the experimental data by solving the parametric identification problem described by the relations (14-17) using Matlab®. It is worth noting that the equations (14-17) represent the non-linear least square, data-fitting problem, which was solved using the Levenberg-Marquardt algorithm. This algorithm was implemented by default in Matlab® using the LSQNONLIN solver. The experimental conditions are presented in Table 4. The parameters  $b_k, k = 0 \dots 3$  of the kinetic model for water adsorption within the composite, which is described by equation (14), are presented in Table 4. The comparison of the experimental kinetic coefficient  $\bar{k}_{o,l}$ , calculated with equation (17) with the kinetic model  $\hat{k}_o$  and described by equation (14), is presented in Figure 7.

**Table 4** Reference conditions used in hydration experiments.

Condition	Experiment 1	Experiment 2	Experiment 3
Mass of anhydrous composite (kg)	2.2	2.1	2.0
Initial water uptake (g/g)	<0.01	0.08	0.13
Air volume flow rate (m <sup>3</sup> /h)	100	100	100
Air temperature at reactor inlet (°C)	17.1	10.0	9.5
Air humidity (kg/kg)	$6.0 \times 10^{-3}$	$5.1 \times 10^{-3}$	$3.4 \times 10^{-3}$
Water vapor pression (Pa)	980	820	550

**Table 5** Numerical values of the parameters of the kinetic model.

Parameter	Value	Units
$b_0$	$3.183 \times 10^{-4}$	1/s
$b_1$	0.330	kg/kg
$b_2$	90.303	--
$b_3$	0.3253	--

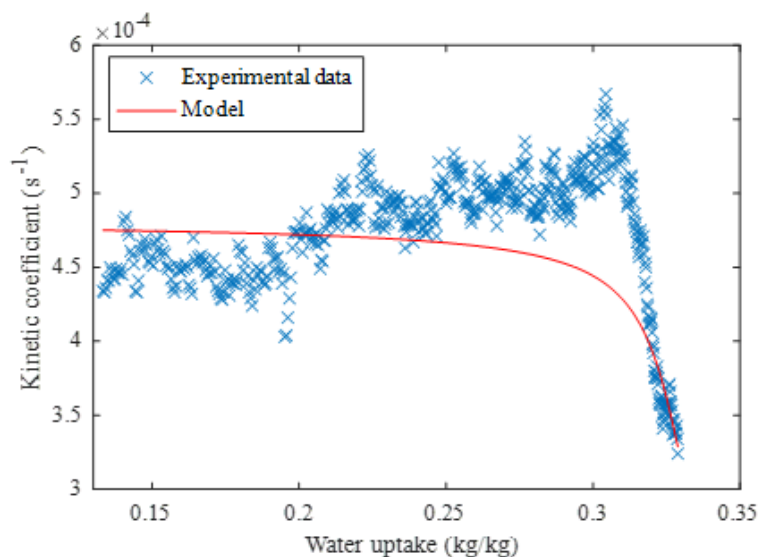


**Figure 7** Validation of the kinetic model on the experimental dataset.

The analysis of the experimental data shown in Figure 7 demonstrates that the kinetic coefficient depends on the water uptake in a non-linear manner. At the beginning of the hydration process, when the water uptake is lower than 0.20 kg/kg, the kinetic coefficient remains a constant around  $4.5 \times 10^{-4}$  1/s. It raises in a step-wise manner to  $4.8 \times 10^{-4}$  1/s in the range of water uptake between 0.20 and 0.25 kg/kg, and then to  $5.1 \times 10^{-4}$  1/s when the water uptake ranges from 0.25 to 0.30 kg/kg. Afterward, there is a sharp drop in the kinetic coefficient when the water uptake becomes greater than 0.30 kg/kg. Such non-linear behavior is due to the changes that occurred in the sorption mechanism. The determination of the exact cause of such a drift requires additional research on the hydro-thermal characteristics of the composite. Nevertheless, the proposed kinetic model allows the apparent kinetic coefficient to be reproduced by the sigmoid-shaped curve on account of the sharp descending front that appears at 0.30 kg/kg of the water uptake.

With the account of identified values for both the heat transfer and kinetic coefficients, the comparison of the model with the experimental data is shown in Figure 8, Figure 9 and Figure 10. The model described in equations (5-10) was implemented and solved in Matlab® by using the ODE15i numerical algorithm to solve a set of differential equations coupled to differential-algebraic equations. The first and second derivatives over the spatial domain that are shown in Figure 5 were calculated by using three-point, second-order, finite difference approximations [22].

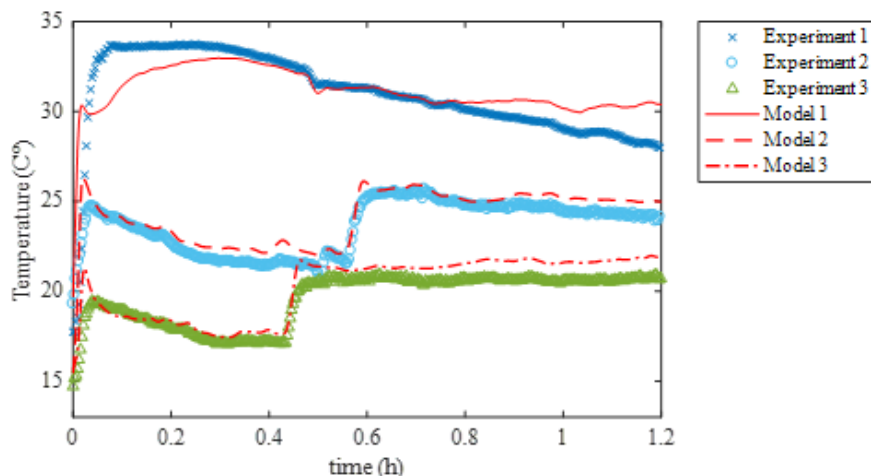


Figure 8 Air temperature at the outlet of the reactor.

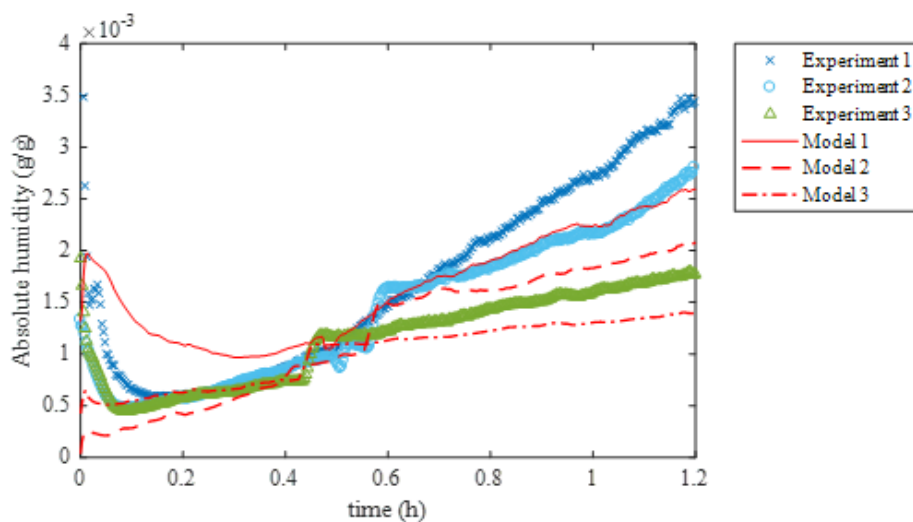


Figure 9 Absolute air humidity at the outlet of the reactor.

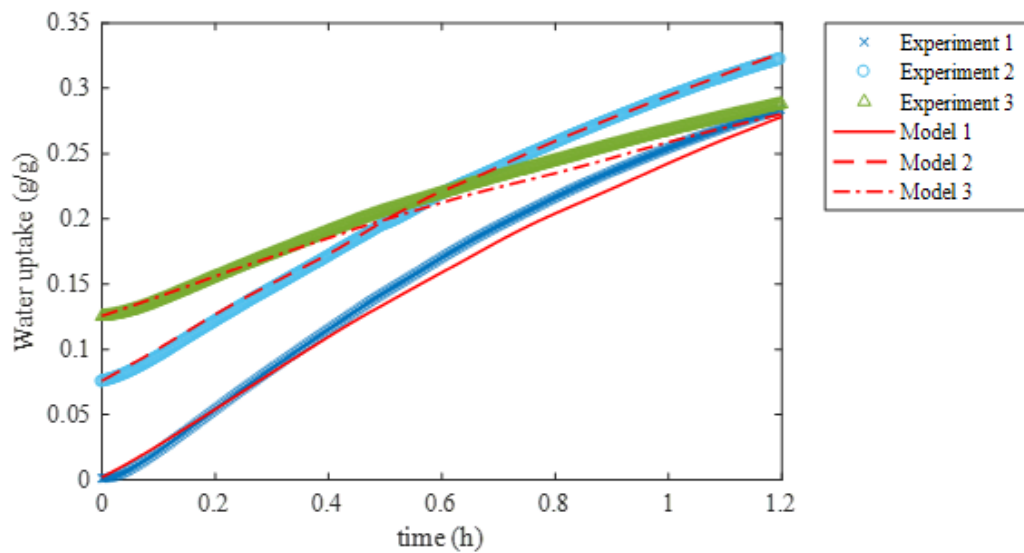


Figure 10 Average water uptake in the composite material.

The validity of this model was verified by calculating the relative root-mean-squared error (RRMSE) shown as follows:

$$RRMSE = \sqrt{\frac{\sum_j (Z_{E,j} - Z_{M,j})^2}{\sum_j (Z_{E,j})^2}} \times 100\% \tag{22}$$

Here,  $Z_{E,j}$  is experimental data and  $Z_{M,j}$  is the model output.

The curves denoted as “Model 1”, “Model 2” and “Model 3” correspond to the respective number of the experiment taken from Table 4. The summary of the comparison of the model against the experimental data is presented in Table 6.

**Table 6** Summary of the model validation on experimental data.

Result	Experiment 1		Experiment 2		Experiment 3		RRMSE (%)
	Measured	Modelled	Measured	Modelled	Measured	Modelled	
Water uptake (kg/kg)	0.29	0.29	0.34	0.36	0.33	0.33	3.6
Maximal thermal power (W)	550	499	471	476	307	305	6.5
Average thermal power (W)	384	401	309	350	173	208	10.8
Thermal energy produced (kWh)	0.48	0.51	0.43	0.49	0.30	0.36	12.7
Energy storage density (kWh/m <sup>3</sup> )	158	163	143	151	102	108	4.7

As shown in Figure 8, Figure 9 and Figure 10, the model predicts the dynamics of the hydration process in the composite with high reliability. The quality of prediction for various curves and performance indicators is slightly different. Despite some differences, a high global prediction performance (see Table 6) of the model was noted since the relative root-mean-squared error (RRMSE) between the measured and modeled values was rather small and varied from 2.1% to at most 12.7%. Therefore, the model is valid and can be used for dynamic simulations.

### 3.2 Dynamic simulations of Typical Days

The hydration process model in the composite, which represents one storage module in the reactor for simulation, was integrated into the TRNSYS (denoted as a “Reactor”). The entire combined solar thermal system is shown in Figure 6. The conditions for simulation are presented in Table 7.

**Table 7** Simulation conditions used for the simulation of the combined solar system.

Condition	Value
Geographic position	Brussels, Belgium
Daily hot water consumption	217 L per day
Water temperature at the tank inlet	10 °C
Temperature range of hot water consumption	From 40 to 55 °C
Position of solar thermal collectors	South, tilt about 40°

The selection of technical parameters, as well as the sizing of components (Table 8), was carried out to achieve the fractional solar coverage for above 70%. The solar collectors allow the water tank to be charged to the maximum cut-off temperature  $T_{SC}^{max}$  which is set to 95 °C. The number of storage modules in the reactor is equal to 2, which represents the compromise between the energy demand and energy production by the thermochemical system with an account of the cut-off values from the control laws present in the equations (17, 18). It was supposed that the minimum cut-off of the air humidity  $w_v^{min}$  and air temperature  $T_a^{min}$  were  $5.0 \times 10^{-3}$  kg/kg and 5 °C, respectively, which meant that the reactor was switched off when one of the cut-off values was detected. At the same time, the maximum admissible charging temperature by the reactor  $T_{DHW}^{max}$  was set as 48 °C, because taking into account the water uptake in non-equilibrium practical conditions, the energy storage density of the material above 40 °C is below 100 kWh/m<sup>3</sup>. When the air temperature at the reactor inlet exceeds 30 °C, the storage modules must be replaced frequently to keep the water tank charged, which results in high demand for the solid. It was found that the reasonable minimum water uptake  $x_s^{min}$  must be not lower than 0.07 kg/kg before the modules are replaced. To restart the reactor, the switching hysteresis  $\Delta T_{bl}$  was set to 2 °C.

**Table 8** Technical parameters used in the simulations.

Component	Value
<u>Solar thermal system</u>	
Total number of solar collectors	5
Net surface area	12.5 m <sup>2</sup>
Water flow rate of the “SC Pump”	300 kg/h
<u>Thermochemical system</u>	
Number of storage modules in the reactor	2
Anhydrous solid mass per 1 module	13 kg
Air flow rate of the fan	968 kg/h
Water flow rate of the pump “R Pump”	235 kg/h
Efficiency of the heat exchangers HX1 et HX2	0.9

<u>Hot water storage tank</u>	
Tank volume	300 l
<u>Back-up thermal system</u>	
Gas burner	1000 W

The overall control algorithm works as follows: The reactor starts to charge the cool-water storage tank during the night. As soon as the average water temperature  $\bar{T}_{DHW}$  in the tank starts to reach the cut-off temperature  $T_{DHW}^{max}$  of 48 °C, the daily frequency of the solid replacement  $\gamma_s(t)$  starts to rise, and the average water uptake in all the storage modules starts to drop down to the cut-off value of  $x_s^{min}$  of 0.07 kg/kg. Afterward, the reactor is switched off, and the charging of the water storage tank is continued by the solar thermal collectors. It must be noted that the solar collectors allow the water storage tank to be charged independently from the thermochemical system as long as there is sufficient solar irradiance. On account of this control logic, the frequency of replacement of the storage modules can vary from 3 to 5, which corresponds to the solid demand, which is at most 130 kg per day.

Given the complexity of the proposed technical system, which is composed of several adjacent sub-systems such as the solar thermal system, thermochemical system, and back-up thermal device, it is extremely difficult to analyze the simulation results every year. Because of the coupling of various components, each having its dynamic behavior, and control laws, it is necessary to simplify the analysis of system dynamics for the sake of determining the most significant factors. Such a simplification is possible during the days that have a typical climate. Moreover, the dynamic behavior of the thermochemical energy storage is made the focus of the present study. The climate data includes many variables. The selection of the climatic conditions is not a trivial task, given that there exists a huge number of possible combinations between these variables. In the context of the study of the dynamic behavior of thermochemical energy storage, the most important climate variables are air temperature and air humidity. The days having a typical climate have climatic conditions that are defined as having a high probability of occurrence for the thermochemical energy storage system to be active during the year. For demonstration, three typical days denoted as ‘cold day’, ‘mild day’, and ‘warm day’ are selected, for which the dynamic behavior of the combined solar system was simulated. The selection of the typical days was performed when the values of both the air temperature and air humidity occurred not less than 16 h during each calendar day. The 16 h duration corresponds to the probability of occurrence of not less than 67% of the air temperature and air humidity, which also ensures a 100% probability for the thermochemical system to be activated. The typical days along with the temperature and air humidity range that are chosen for the simulations, are presented in Table 9.

**Table 9** Typical climate days used in dynamic simulations of the combined solar system.

Notation	Representative Date	Temperature range (°C)	Air humidity range (kg/kg)	Probability $\times 10^{-3}$
----------	---------------------	------------------------	----------------------------	------------------------------

“Cold day”	31 October	2.71 ... 8.27	4.57 ... 7.8	70%
“Mild day”	14 April	8.27 ... 13.8	4.57 ... 7.8	82%
“Warm day”	29 May	13.8 ... 19.4	4.57 ... 7.8	22%

It must be noted that the probability of occurrence of a so-called “warm day” is only 22%, despite wide ranges of air temperature and air humidity. However, in the mild climate of Brussels location (Belgium), this condition usually coincides with rainy and cloudy days, which almost excludes the participation of the solar collectors from the tank charging process. It is clear that with the limitations imposed by the control laws, the thermochemical energy storage system would not be able to charge the water storage tank beyond 48 °C, and the back-up thermal device will automatically be activated in place of the solar thermal collectors. The simulation results are discussed here below and are shown in Figure 11, 12, ..., 19. The curves denoted as “Tank Node 1-5” represent the temperature of water at specific points within the water storage tank along the vertical axis, which were modeled using the TRNSYS software. The curve “Hot Water Temperature” represents the domestic hot water consumption profile. The curve “Reactor Temperature” is regarding the air temperature at the reactor outlet. The curve “Solar Collectors Temperature” represents the temperature of the fluid at the outlet of the solar thermal collectors.

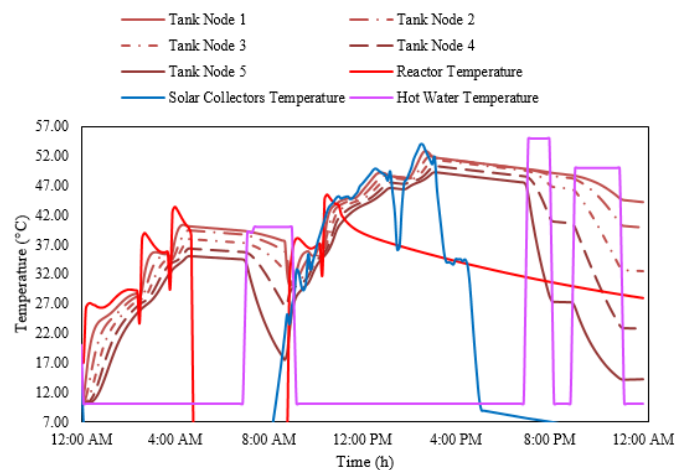


**Figure 11** Temperature profiles in the combined solar system during a “cold day”.

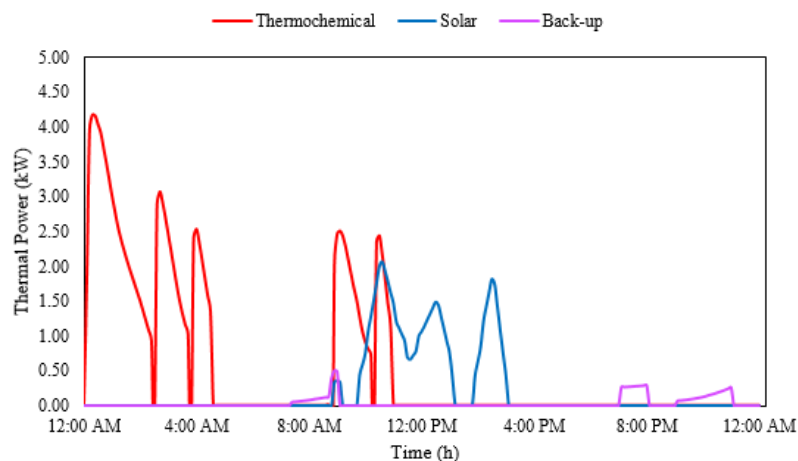


**Figure 12** Thermal power profiles in the combined solar system during a “cold day”.

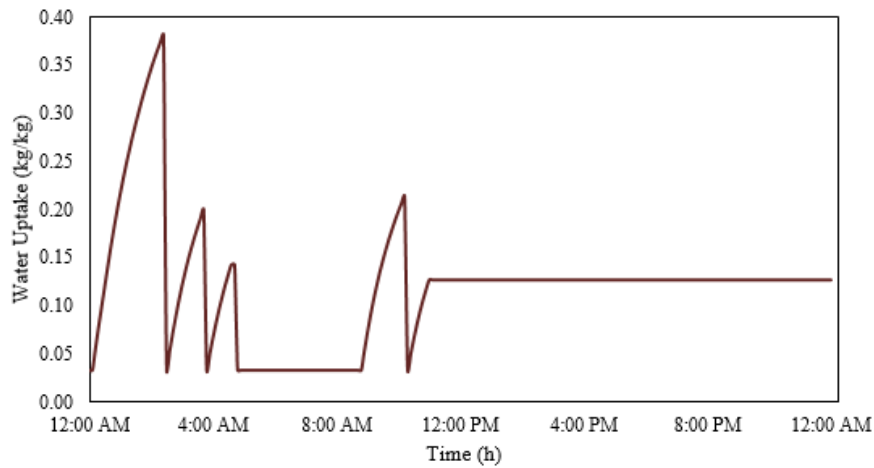


**Figure 13** Water uptake in the solid during a “cold day”.

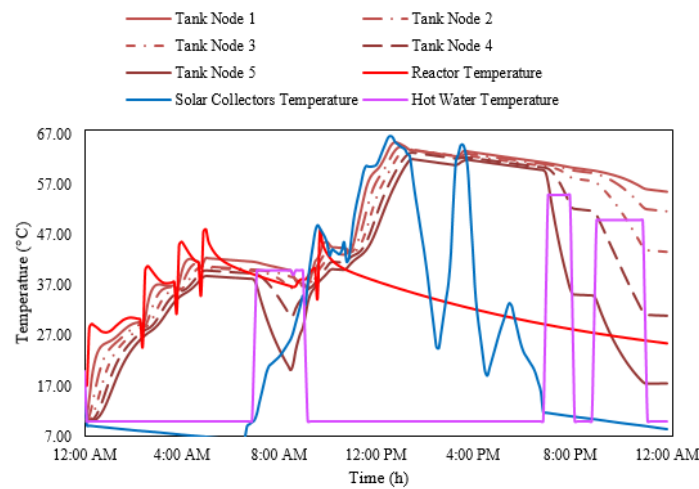


**Figure 14** Temperature profiles in the combined solar system during a “mild day”.

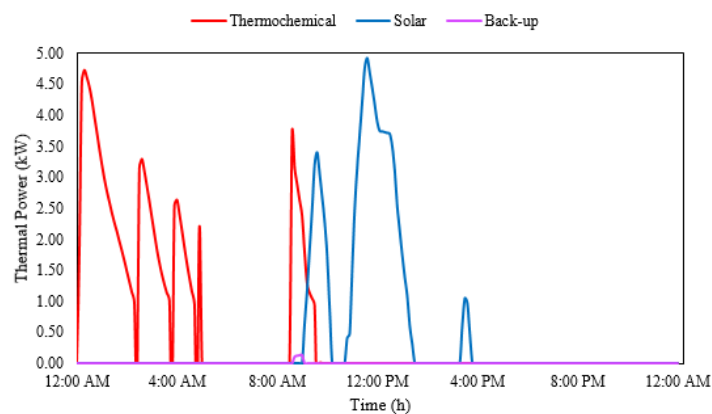


**Figure 15** Thermal power profiles in the combined solar system during a “mild day”.

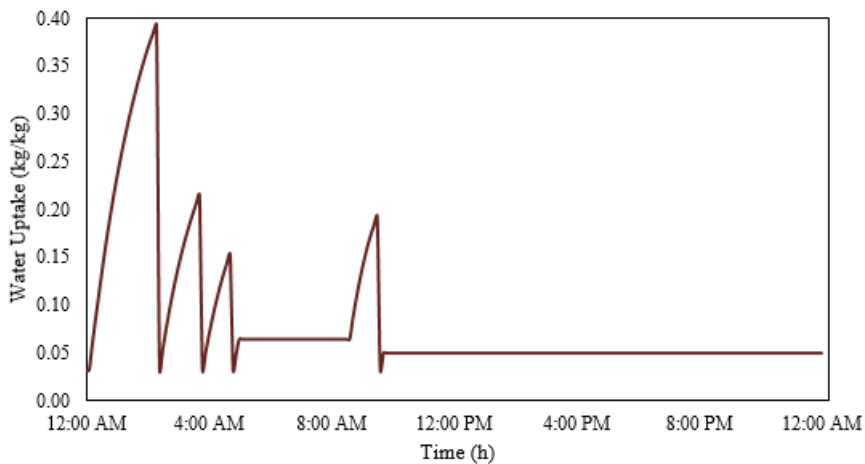


**Figure 16** Water uptake in the solid during a “mild day”.

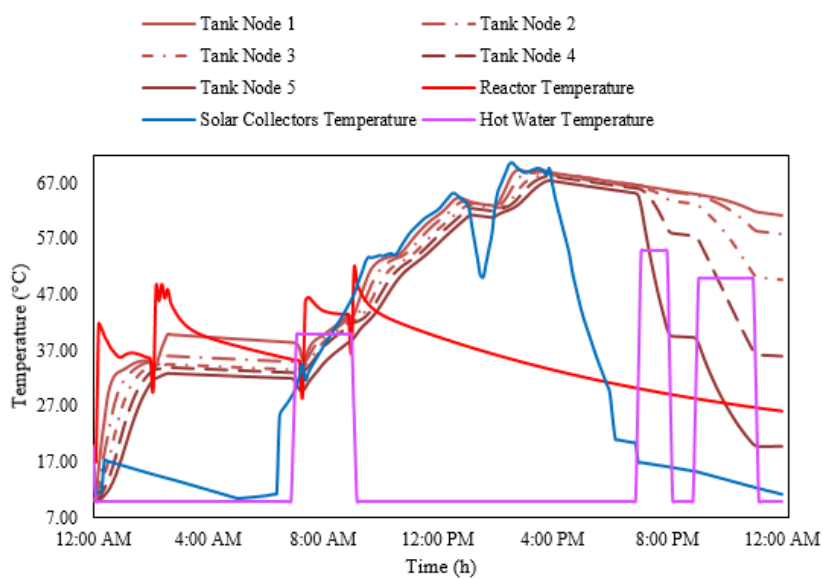


**Figure 17** Temperature profiles in the combined solar system during a “warm day”.

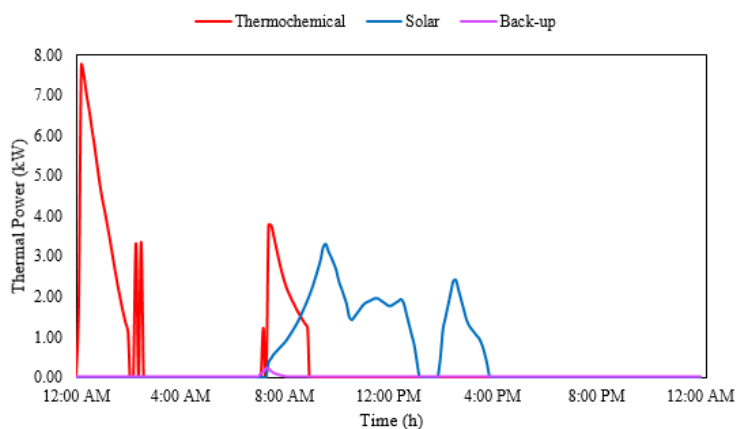


**Figure 18** Thermal power profiles in the combined solar system during a “warm day”.

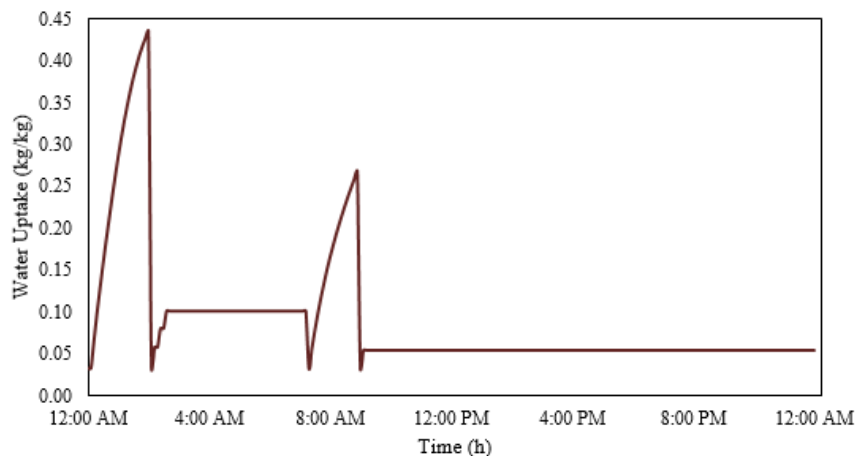


**Figure 19** Water uptake in the solid during a “warm day”.

### 3.2.1 Simulation of a “Cold Day”

This typical day is characterized by the air temperature fluctuating between 3 °C and 10 °C, whereas the air humidity remains at about  $5.2 \times 10^{-3}$  kg/kg. The water storage tank starts charging from 10 °C by the thermochemical reactor. The temperature in the tank rises to 40 °C during 4 h before the early consumption of hot water, which starts at 6:00 am (see Figure 11). Between 4:00 and 6:00 am, the combined system is halted because the maximum achievable temperature is limited to 48 °C. The temperature in the water storage tank is maintained at 40 °C at the top layer (see Figure 11). The maximal thermal power injected by the thermochemical system in the water tank reduces from 4.15 kW to 2.5 kW along with the thermal charge of the tank due to the natural decrease of the adsorption capacity related to the water sorption equilibrium (see Figure 12). The working cycle of the reactor becomes shorter after every solid replacement. The average water uptake in the solid also reduces from 0.38 kg/kg to 0.14 kg/kg (see Figure 13). As a result, the energy storage density in the solid already drops down from 214 kWh/m<sup>3</sup> to 79 kWh/m<sup>3</sup> during the first 4 h of charging of the tank. Some amount of heat lesser than 500 W is supplied by the back-up thermal device at 6:00 am to compensate for a small amount of thermal loss in the water tank (see Figure 12). At 8:00 am, all adjacent systems work simultaneously. Technically, this is not a conflictual situation; however, the control algorithm must be improved to avoid this type of situation. The thermal charging of the water storage tank is prioritized by the solar collectors from 9:00 am to 3:00 pm so that the temperature in the tank increases up to 50 °C (see Figure 11). The thermochemical reactor is deactivated from 5:00 pm because the air humidity drops below the cut-off limit of  $5.0 \times 10^{-3}$  kg/kg. The back-up thermal device is activated from 7:00 pm to 9:00 pm (see Figure 12), supplying at most 380 W of the thermal power.

### 3.2.2 Simulation of a “Mild Day”

This typical climate day is characterized by the variation in the air temperature ranging from 6.4 °C to 14.3 °C. The air humidity fluctuates within the range of  $5.6 \times 10^{-3}$  kg/kg to  $6.4 \times 10^{-3}$  kg/kg. Similarly, the charging of the water tank is ensured by the thermochemical reactor from 0:00

am to 5:00 am until the temperature in the top layer of the tank reaches 42.3 °C and the temperature at the reactor outlet crosses the cut-off limit (see Figure 14). During this period, the thermal power at the outlet of the thermochemical system reduces from 4.5 to 2.2 kW (see Figure 15), and the solid in the reactor is replaced four times before using the hot water (see Figure 16). The energy storage density of the material reduces from 221.5 kWh/m<sup>3</sup> after the first replacement to 86.5 kWh/m<sup>3</sup> after the third replacement. The fourth reactor switching cycle occurs at about 4:45 am. However, the reactor works only for 12 min before the temperature at the outlet of the reactor reaches the cut-off limit. In such conditions, the water uptake is as high as 0.064 kg/kg. The reactor is temporarily stopped, and then it restarts later at 8:35 am. The final water uptake is about 0.19 kg/kg, while the energy storage density in the solid is 108.8 kWh/m<sup>3</sup>. It must be noted that the reactor is switched on for the fifth time at 9:00 am (see Figure 15 and Figure 16), but the control algorithm does not allow the reactor to run in the present conditions. The next working cycle is postponed to the next day. The solar collectors continue the thermal charge of the water storage tank from 9:00 am to 3:00 pm. The peak thermal power attains 4.92 kW at 11:00 am (see Figure 15). The amount of thermal energy produced by the solar collectors is high enough to charge the water tank up to 63 °C. The back-up heater is only used for 25 min to compensate for the difference of about 130 W (see Figure 15).

### 3.2.3 Simulation of a “Warm Day”

In this case of simulation, the air temperature varies within the range of 10.2 °C to 19.1 °C, while the air humidity ranges from  $6.6 \times 10^{-3}$  kg/kg to  $9.8 \times 10^{-3}$  kg/kg. First, the control algorithm activates the thermochemical system that works till 2:30 am. By this time, the temperature of water at the top layer of the tank reaches 40 °C (see Figure 17). Such a prompt rise in temperature is due to the high humidity content, which is  $9.0 \times 10^{-3}$  kg/kg, which leads to the high equilibrium uptake (see adsorption isotherm curves in Figure 3) and to a high thermal power output by the reactor. Indeed, the thermal power reaches 7.7 kW (see Figure 18). Under such a condition, the water uptake in the solid is as high as 0.44 kg/kg, while the energy storage density in the solid is 247.3 kWh/m<sup>3</sup>. It is worth noting that the high humidity content results in the frequent on/off switching of the reactor (see Figure 17, Figure 18 and Figure 19). The reactor works under unfavorable conditions because the water uptake in the solid reaches only 0.1 kg/kg and because the energy storage density of the material is only 56.2 kWh/m<sup>3</sup>. The reactor continues to work around 7:20 am for 1.7 h (see Figures 17, Figure 18 and Figure 19). All three adjacent systems are activated simultaneously for 1.2 h (see Figure 18). The thermal power produced by the back-up heating device is limited by 214 W at most. Afterward, the solar collectors constitute a major part of the daily energy demand. The water temperature in the storage tank reaches 68 °C around 2:00 pm. Finally, the solar collectors are deactivated after 4:00 pm, leaving the water tank to be fully charged till the end of the day (see Figure 17).

### 3.3 Summary of Energy Performance

The overview of the simulation results is presented in Table 10 in the form of performance indicators. The performance indicators for the thermochemical system were calculated using equations (1-4). The amount of energy produced by the solar collectors and back-up heater was

determined with the help of TRNSYS by using the built-in integrator function plugged into the concerned component, as shown in Figure 6.

**Table 10** Summary of the simulation results for the combined solar system under days of typical climate.

Performance indicator	Value		
	“Cold day”	“Mild day”	“Warm day”
<u>Thermochemical system</u>			
Thermal energy produced by the system (kWh)	12.95	12.94	12.66
Total solid mass (kg)	130	104	78
Energy storage density in the solid per lot (kWh/m <sup>3</sup> ):			
- lot 1	214.7	221.5	247.3
- lot 2	112.1	121.1	56.2
- lot 3	79.4	86.5	150
- lot 4	119.4	108.8	--
- lot 5	71	--	--
<u>Solar thermal system</u>			
Thermal energy produced by the system (kWh)	5.4	10.4	12.8
<u>Back-up thermal system</u>			
Energy supplement produced by the system (kWh)	0.87	0.05	0.11

It is worth noting that a “lot” comprises the solid mass contained in each storage module in the reactor. The actual model accounts for the homogeneous water sorption in the solid material, and therefore the average water uptake remains equal in each of the storage modules. The amount of thermal energy produced by the thermochemical system is almost in the same order for each typical day and varies from 12.66 to 12.95 kWh. Such an insignificant difference can be related to the cut-off temperature limit of the reactor, which was set as 48 °C. Despite this fact, the replacement frequency of the lot is not the same, and it depends on the air temperature and air humidity at the inlet of the reactor. During the “cold day”, the air humidity used during the simulation was about  $5.2 \times 10^{-3}$  kg/kg, and the air temperature was below 10 °C. Under such a circumstance, the temperature at the reactor outlet cannot reach the cut-off temperature, which results in a high frequency of solid replacement. On the contrary, during a “warm day”, the reactor works under conditions with relatively high humidity content and air temperature, which results in the high output of thermal power and high switching frequency of the reactor. For this kind of condition, the parameters in the control law in equation (17) must be respectively adjusted in such a manner to avoid frequent on/off running cycles in the reactor. This means that the cut-off temperature of the reactor must be placed higher than 48 °C. At the same time, the cut-off temperature must be

lowered during conditions of little humidity content in the air to avoid too many replacements of lots.

It is important to address the disinfection problem of the water storage tank. The growth of pathogens in the water storage tank and water distribution system requires special studies, including the collection of experimental data and validation of the thermal management algorithm. This topic was not included in the present study because the primary focus was on the determination of the energy performance characteristics of the thermochemical reactor. Nevertheless, basic conditions and measures were taken for the thermal disinfection of the water storage tank, because the water temperature in the tank was periodically heated above 60 °C (see Figure 14 and Figure 17).

#### 4. Conclusions

In this paper, the prototype of the combined solar thermochemical system was fully built and instrumented. The single storage module filled with 2.2 kg of composite thermochemical material was experimentally tested. The energy storage density in the material under experimental non-equilibrium conditions varied between 102 and 158 kWh/m<sup>3</sup>. The average thermal power was measured as high as 384 W for the range having a higher air humidity, and it was about 173 W for the range having a lower air humidity. These numbers showed great applied interest for the validation of the theoretical model of the adsorption process. The validation of the mathematical model for the adsorption of water vapor in a composite was carried out. It was concluded that the proposed kinetic model was valid and allowed the dynamics of the adsorption process to be predicted with high reliability. Finally, the simulator of the combined system was built using the TRNSYS software. The study of the thermal charge of the water storage tank for domestic hot water production was performed under conditions represented during typical climatic days. It was found that the performance indicators highly depended on the control algorithm, especially for thermochemical energy storage. Additional research about the improvement of the control algorithm is required.

#### Nomenclature

---

<u>Abbreviations</u>			
BTD	Back-up thermal device	P	Hydraulic pump
DHW	Domestic hot water	SC	Solar thermal collectors
F	Fan	SM	Storage module
HX	Heat exchanger	RRMSE	Relative root-mean squared error
<u>Symbols</u>			
$a, b$	Constants	$\mu$	Dynamic viscosity (Pa/s)
$C_p$	Heat capacity (W/kg/K)	$Nu$	Nusselt number
$D_L$	Diffusivity (m <sup>2</sup> /s)	$Pr$	Prandtl number
$\Delta$	Difference operator	$p$	Partial gas pressure (Pa)
$\Delta E_r$	Energy storage density (kWh/m <sup>3</sup> )	$\dot{Q}$	Thermal power (W)
$\Delta H_s$	Reaction heat (J/kg)	$Re$	Reynolds number
$E$	Energy (kWh)	$\rho$	Specific mass (kg/m <sup>3</sup> )

$\varepsilon$	Porosity	$S$	Sutherland constant (K)
$\gamma$	Logical variable	$T$	Temperature (°C)
$h_0$	Heat transfer coefficient (W/K)	$t$	Time (s)
$k_o$	Kinetic coefficient (1/s)	$u$	Linear velocity (m/s)
$\lambda_L$	Thermal diffusivity (m <sup>2</sup> /s)	$w$	Air humidity (kg/kg)
$M$	Molar mass (kg/mol)	$X_m$	Molar fraction (mol/mol)
$m$	Mass (kg)	$x$	Water uptake (kg/kg)
$\dot{m}$	Mass flow rate (kg/s)	$x_s^0$	Adsorption equilibrium (kg/kg)
$Z$	Denotes data in a data vector		

### Subscripts

a	Refers to air	M	Refers to modeled data
bed	Indicates storage module (bed)	out	Indicates output
BTD	Indicates back-up thermal device	p	Refers to the particle characteristics
DHW	Refers to domestic hot water	r	Refers to thermochemical reactor
E	Refers to experimental data	s	Refers to solid material
g	Refers to gas mixture	SC	Refers to solar thermal collectors
in	Indicates input	v	Refers to water vapor

### Superscripts

0	Indicates reference equilibrium state	or min	Minimum threshold
max	Maximum threshold		

---

## Acknowledgments

Authors thank the BESOL (Rochefort, Belgium) team for the partnership in manufacturing and mounting of the prototype. Authors acknowledge Solvay for the provision of Caso® granules.

## Author Contributions

Conceptualization, methodology, writing original draft, O.S.; Composite material curation, E.C.; Visualization, validation, writing review and editing, E.C., N.H., M.F.; Conceptualization, supervision, project administration, funding acquisition, M.F.

## Funding

This research was funded by European Regional Development Fund and Wallonia Region, project reference FEDER C3E2D–STOCC.



## Competing Interests

The authors have declared that no competing interests exist.

## References

1. Rockenfeller V, Kirol LD, Ryan WA. Solid-gas chemisorption; efficient HVAC and R without CFCs. *ASHRAE J.* 1992; 34: 54-58.
2. Srivastava NC, Eames IW. A review of adsorbents and adsorbates in solid-vapour adsorption heat pump systems. *Appl Therm Eng.* 1998; 18: 707-714.
3. Clark RJ, Mehrabadi A, Farid M. State of the art on salt hydrate thermochemical energy storage systems for use in building applications. *J Energy Storage.* 2020; 27: 101145.
4. Scapino L, Zondag HA, Van Bael J, Diriken J, Rindt CC. Energy density and storage capacity cost comparison of conceptual solid and liquid sorption seasonal heat storage systems for low-temperature space heating. *Renew Sust Energ Rev.* 2017; 76: 1314-1331.
5. Pinheiro JM, Salústio S, Rocha J, Valente AA, Silva CM. Adsorption heat pumps for heating applications. *Renew Sust Energ Rev.* 2020; 119: 109528.
6. Roumpedakis TC, Kallis G, Magiri-Skouloudi D, Grimekis D, Karellas S. Life cycle analysis of ZEOSOL solar cooling and heating system. *Renew Energ.* 2020; 154: 82-98.
7. Wang RZ, Li M, Xu YX, Wu JY. An energy efficient hybrid system of solar powered water heater and adsorption ice maker. *Sol Energy.* 2000; 68: 189-195.
8. Ji X, Song X, Li M, Liu J, Wang Y. Performance investigation of a solar hot water driven adsorption ice-making system. *Energy Convers Manag.* 2015; 106: 759-765.
9. Zhao YJ, Wang RZ, Li TX, Nomura Y. Investigation of a 10 kWh sorption heat storage device for effective utilization of low-grade thermal energy. *Energy.* 2016; 113: 739-747.
10. Zhang Y, Wang R. Sorption thermal energy storage: Concept, process, applications and perspectives. *Energy Stor Mater.* 2020; 27: 352-369.
11. Gaeini M, van Alebeek R, Scapino L, Zondag HA, Rindt CC. Hot tap water production by a 4 kW sorption segmented reactor in household scale for seasonal heat storage. *J Energy Storage.* 2018; 17: 118-128.
12. Michel B, Mazet N, Neveu P. Experimental investigation of an open thermochemical process operating with a hydrate salt for thermal storage of solar energy: Local reactive bed evolution. *Appl Energy.* 2016; 180: 234-244.
13. Aydin D, Casey SP, Chen X, Riffat S. Novel "open-sorption pipe" reactor for solar thermal energy storage. *Energy Convers Manag.* 2016; 121: 321-334.
14. Bertsch F, Jaehnig D, Asenbeck S, Kerskes H, Drucek H, Wagner W, et al. Comparison of the thermal performance of a solar heating system with open and closed solid sorption storage. *Energy Procedia.* 2014; 48: 280-289.
15. Palomba V, Frazzica A. Comparative analysis of thermal energy storage technologies through the definition of suitable key performance indicators. *Energy Build.* 2019; 185: 88-102.
16. Skrylnyk O, Courbon E, Heymans N, Frere M, Bougard J, Descy G. Performance characterization of salt-in-silica composite materials for seasonal energy storage design. *J Energy Storage.* 2018; 19: 320-336.
17. Wyttenbach J, Bougard J, Descy G, Skrylnyk O, Courbon E, Frère M, et al. Performances and modelling of a circular moving bed thermochemical reactor for seasonal storage. *Appl Energy.* 2018; 230: 803-815.
18. Courbon E, D'Ans P, Permyakova A, Skrylnyk O, Steunou N, Degrez M, et al. Further improvement of the synthesis of silica gel and CaCl<sub>2</sub> composites: Enhancement of energy storage density and

stability over cycles for solar heat storage coupled with space heating applications. Sol Energy. 2017; 157: 532-541.

19. Pearson JR. A note on the “Danckwerts” boundary conditions for continuous flow reactors. Chem Eng Sci. 1959; 10: 281-284.
20. Wakao N, Funazkri T. Effect of fluid dispersion coefficients on particle-to-fluid mass transfer coefficients in packed beds: Correlation of Sherwood numbers. Chem Eng Sci. 1978; 33: 1375-1384.
21. Buddenberg JW, Wilke CR. Calculation of gas mixture viscosities. Ind Eng Chem Res. 1949; 41: 1345-1347.
22. Bickley WG. Formulae for numerical differentiation. Math Gazette. 1941; 25: 19-27.



Enjoy *JEPT* by:

1. [Submitting a manuscript](#)
2. [Joining in volunteer reviewer bank](#)
3. [Joining Editorial Board](#)
4. [Guest editing a special issue](#)

For more details, please visit:

<http://www.lidsen.com/journal/jept>